*GB ENGN TEC APPL SCI*
Structural Dynamic Systems Computational Techniques
and Optimization Seismic Techniques
Vol. 12, 1-24 (1999)

# 1 TECHNIQUES IN THE NONLINEAR DYNAMIC ANALYSIS OF SEISMIC ISOLATED STRUCTURES

M.C. CONSTANTINOU[1,*], A.M. REINHORN[1], P. TSOPELAS[1] and S. NAGARAJAIAH[2]

[1]*Department of Civil Engineering, State University of New York at Buffalo,*
**Tel: (716) 645-2114 ext. 2404*
*132 Ketter Hall, Buffalo, NY 14260, USA*
[2]*Department of Civil Engineering, University of Missouri-Columbia, Columbia, MO 65211, USA*

## 1.1. INTRODUCTION

In conventional seismic design acceptable performance of a structure during earthquake shaking is based on the lateral force resisting system being able to absorb and dissipate energy in a stable manner for a larger number of cycles. Energy dissipation occurs in specially detailed ductile plastic hinge regions of beams and column bases, which also form part of the gravity load carrying system. Plastic hinges are regions of concentrated damage to the gravity frame, which often is irreparable. Nevertheless, this design approach is acceptable because of economic considerations provided, of course, that structural collapse is prevented and life safety is ensured.

For important structures, such as hospitals, police stations, etc., the conventional seismic design approach may not be applicable. Since these structures must be designed to remain functional after an earthquake, they are typically designed with sufficient strength so that inelastic action is either prevented or minimized. Apart from being a costly design approach, it is often

insufficient in safeguarding against damage or failure of important secondary systems, which are needed for continuing serviceability.

Moreover, a large number of older structures have insufficient lateral strength and lack the detailing required for ductile behavior. Seismic retrofitting of these structures is necessary and may be achieved by conventional seismic design, although often at significant cost and with undesirable disruption of architectural features.

Alternate design procedures have been developed that can, when properly applied, to eliminate or significantly reduce seismic damage to structures. Seismic isolation represents the most effective of these procedures.[1–3] Seismic isolation is based on the premise that it is possible to separate a structure from its foundation through the introduction of a mechanical system which is characterized by rigidity under service loads, and flexibility and energy absorption capability under seismic loads. The system acts as a filter that reflects seismic energy away of the structure, reducing thus seismic inertia forces at the expense, however, of large displacements at the isolation system level. Reduction of these displacements to acceptable levels is accomplished through dissipation of seismic energy.

Seismic isolation is a new technology with relatively few applications, which amount to about 200 buildings and 250 bridges, worldwide. However, these applications mostly involve monumental structures, and for the United States many are retrofit applications for historic buildings. Examples are the Salt Lake City and County Building, Oakland City Hall, U.S. Court of Appeals in San Francisco, San Francisco City Hall, San Bernardino Country Medical Center, New San Francisco International Airport Terminal, Liquefied Natural Gas (LNG) Facility in Greece, C-1 Computer Center Building in Japan and the bridges over the Corinth Canal in Greece. Figure 1 shows a view of the U.S. Court of Appeals building in San Francisco. This five-story, 32,500 $m^2$ floor area building was constructed in 1905. It survived the 1906 San Francisco earthquake but it suffered damage in the 1989 Loma Prieta earthquake. It has been seismically strengthened and isolated by 256 isolation bearings at its foundation.[4] Figure 2 shows a view of the layout of 212 isolation bearings of one of two identical LNG storage tanks during construction in Greece in 1995. The isolation system is located about 20 m under the ground surface. It supports the steel LNG storage tank and a protective prestressed concrete tank of 70 m diameter and 32 m height.

The subject of seismic isolation is described in numerous publications, of which large but not complete lists may be found in the books of Skinner *et al.*[1], Kelly[2] and Soong and Constantinou.[3] These books present the theory, state-of-the-art and state-of-practice in seismic isolation. The present chapter serves the role of addressing the analysis of seismic isolated structures. It primarily describes the work of the authors in the mathematical representation

**Figure 1.** View of U.S. Court of Appeals building in San Francisco.

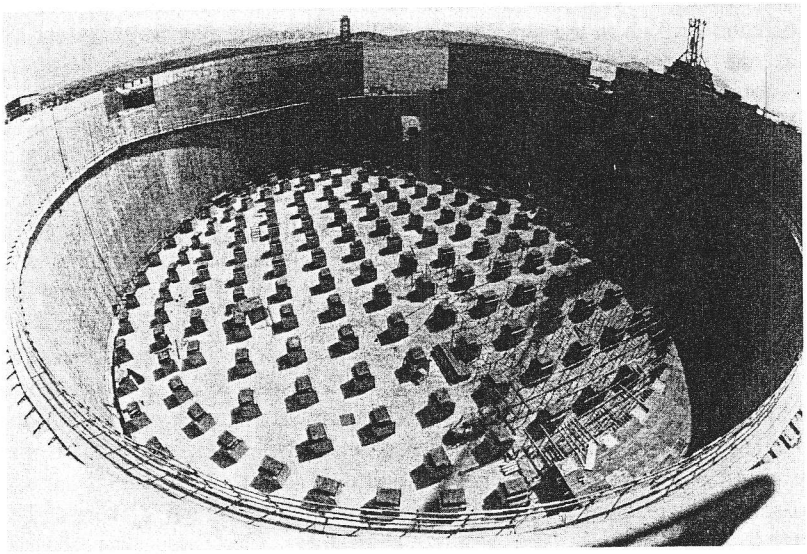

**Figure 2.** View of isolated LNG storage tank facility under construction in 1995.

of seismic isolation hardware and in the development of the class of computer codes 3D-BASIS for the nonlinear dynamic analysis of isolated structures.

## 1.2. SEISMIC ISOLATION HARDWARE, BEHAVIOR AND MATHEMATICAL REPRESENTATION

The basic elements in a practical seismic isolation system are flexibility to lengthen the period and produce the isolation effect, energy dissipation capability to reduce displacements to practical design levels, and means for rigidity under service loads. Examples of practical isolation systems are high damping elastomeric bearings, lead-rubber bearings, elastomeric bearings in combination with energy dissipating devices and sliding bearings with or without restoring force capability.

### 1.2.1. Elastomeric Bearings

Elastomeric bearings represent a common means for introducing flexibility into and isolated structure. Figure 3 shows the construction of two such bearings. They consist of thin layers of natural rubber which are vulcanized and bonded to steel plates. Natural rubber exhibits a complex mechanical behavior, which in the simplest possible description may be characterized as one of combined viscoelastic and hysteretic behavior. Low damping natural rubber bearings exhibit essentially linear elastic and linear viscous behavior to large shear strains (horizontal displacement divided by total rubber thickness). The equivalent damping ratio is typically less than 0.05 of critical for shear strains in the range of 0 to 200%.[3]

Lead-rubber bearings are constructed of low damping natural rubber with a preformed central hole. A lead core is press-fitted in the hole. Figure 4 shows a lead-rubber bearing cut in half to expose its internal construction. The lead core deforms in almost pure shear, yields at low level of stress (8 to 10 MPa in shear at normal temperature) and produces hysteretic behavior which is stable over a number of cycles. Unlike mild steel, lead recrystallizes at normal temperature (about 20°C), so that repeated yielding does not cause fatigue. Lead-rubber bearings exhibit characteristic strength which ensures rigidity under service loads. Figure 5 shows an idealized force-displacement relation of a lead-rubber bearing. The characteristic strength, $Q$, is related to the lead plug area, $A_p$, and the shear yield stress of lead, $\sigma_{YL}$

$$Q = A_p \sigma_{YL} \tag{1}$$

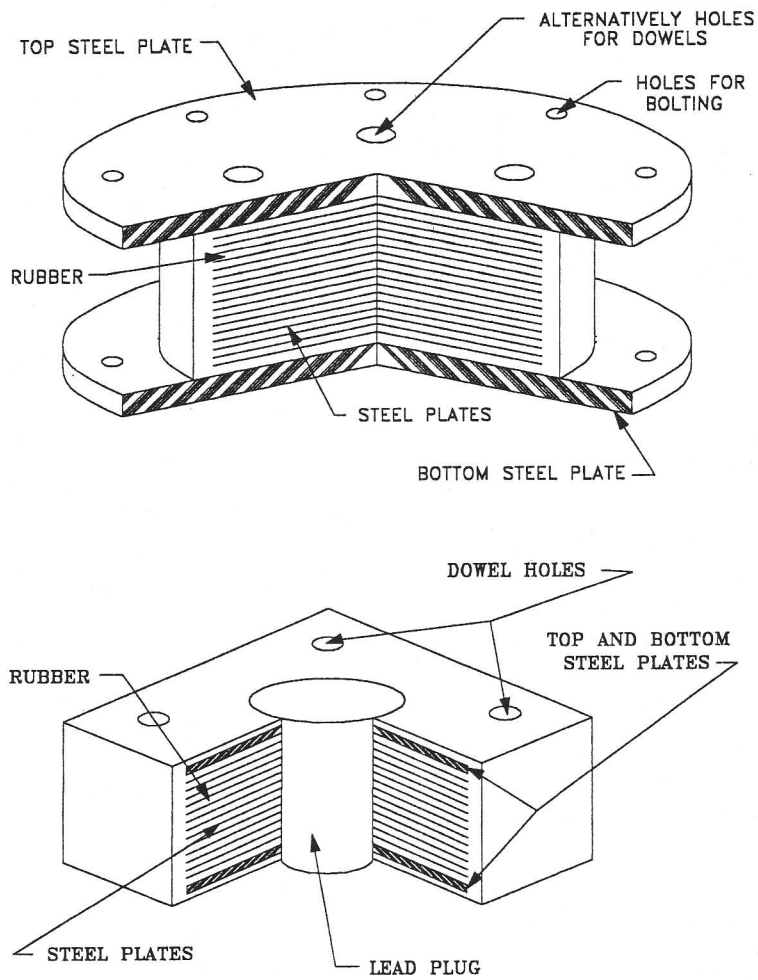


**Figure 3.** Construction of elastomeric bearings.

The post-yielding stiffness, $K_p$, is typically higher than the shear stiffness of the bearing without the lead core:

$$K_p = \frac{A_r G}{\Sigma t} f \tag{2}$$

where $A_r$ is the bonded rubber area, $\Sigma t$ is the total rubber thickness, $G$, is the shear modulus of rubber, and $f$ is a factor larger than unity. Under

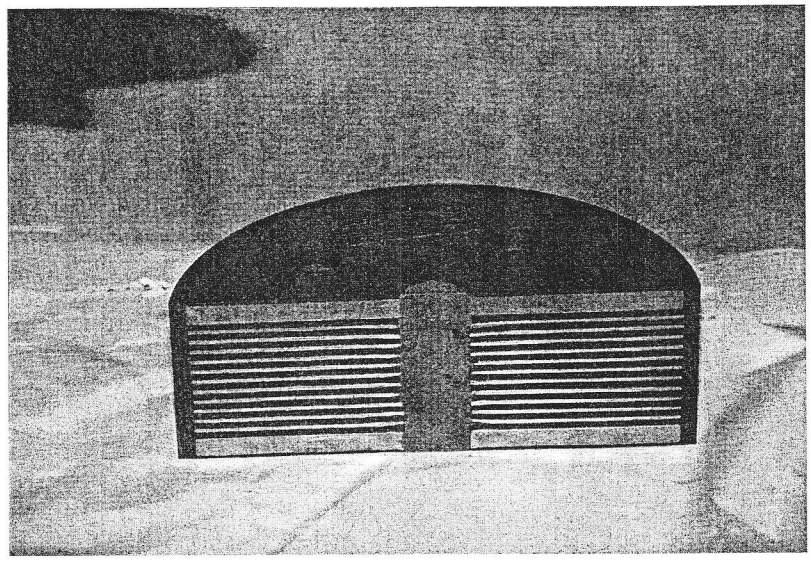

**Figure 4.** View of lead-rubber bearing cut in half to expose internal structure.

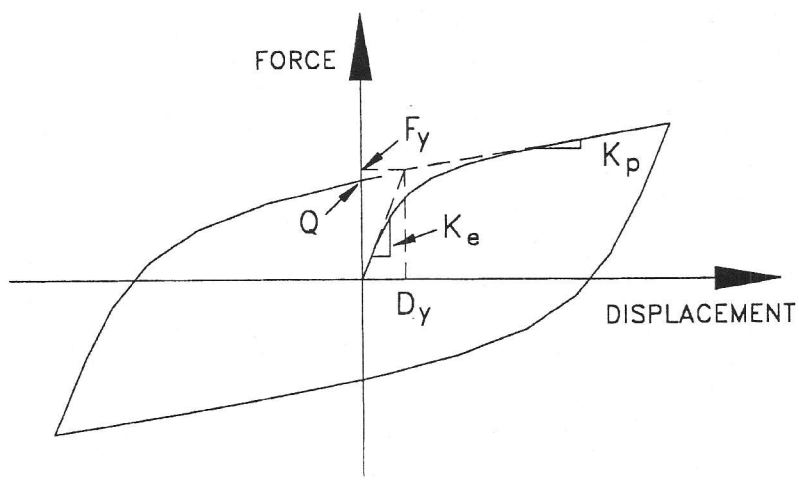


**Figure 5.** Idealized force-displacement relation of elastomeric bearing.

proper conditions, $f$, may be equal to or less than 1.15. Moreover, the elastic stiffness, $K_e$, ranges between 6.5 to 10 times the post-yielding stiffness.

A mathematical model appropriate for modeling hysteretic behavior as that of lead-rubber bearings has been incorporated in the 3D-BASIS class of computer programs for dynamic analysis of isolated structures.[5–7] In this model, the forces along the orthogonal directions which are mobilized during motion of the bearing are described by:

$$F_x = \alpha \frac{F^y}{D_y} U_x (1+\alpha) F^y Z_x, \qquad F_y = \alpha \frac{F^y}{D_y} U_y (1+\alpha) F^y Z_y, \tag{3}$$

in which $\alpha$ is the post-yielding to pre-yielding stiffness ratio, $F^y$ is the yield force and $D_y$ is the yield displacement, as illustrated in Figure 5. $Z_x$ and $Z_y$ are dimensionless variables governed by the following system of differential equations which was proposed by Park *et al.*[8]:

$$D_y \dot{Z}_i + \gamma |\dot{U}_i Z_i| Z_i + \beta \dot{U}_i Z_i^2 + \gamma |\dot{U}_j Z_j| Z_i + \beta \dot{U}_j Z_i Z_j - A \dot{U}_j = 0 \tag{4}$$

where in one equation $i = x$, $j = y$ and in another $i = y$, $j = x$. Parameters $A$, $\beta$ and $\gamma$ are dimensionless and $U_x$, $U_y$, and $\dot{U}_x$, $\dot{U}_y$, represent, respectively, the displacements and velocities that occur at the isolation element. Constantinou *et al.*[9] have shown that when motion commences and displacements exceed the yield displacement, Equation 4 has the following solution provided that $A/(\beta+\gamma) = 1$

$$Z_x = \cos\theta, \qquad Z_y = \sin\theta \tag{5}$$

where $\theta$ is the angle specifying the instantaneous direction of motion

$$\theta = \tan^{-1}(\dot{U}_y/\dot{U}_x) \tag{6}$$

Equations 5 and 6 indicate that the interaction curve of the element is circular.

High damping rubber bearings are made of specially compounded rubber which exhibits equivalent damping ratio of about 0.10 to 0.20 of critical. Figure 6 shows representative force-displacement loops of a small scale bearing (bonded area $A_r = 52258$ mm$^2$, rubber thickness $\Sigma t = 8.25$ mm) under scragged conditions. Scragging is the process of subjecting the bearing to a number of cycles of motion so that certain internal structures of rubber are severed and the bearing attains stable properties with low stiffness. It has been assumed in the past that the scragged properties when attained they become permanent. However, recent studies[10] demonstrated that high damping rubber recovers, either fully or partially, its virgin properties within a short time interval after testing. The extend of recovery depends on the elastomeric compound.

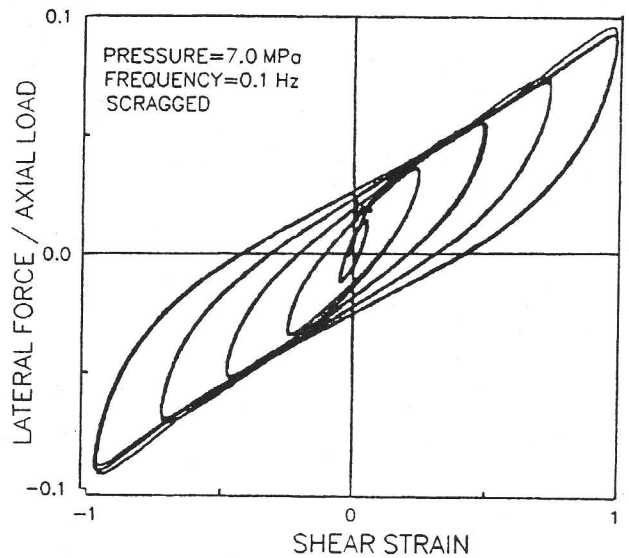


**Figure 6.** Force-displacement loops of high damping rubber bearing.

Mathematical models capable of describing the complex virgin stage to scragged stage properties of high damping rubber bearings are not yet available. It is common to perform multiple analyses with stable hysteretic models and obtain bounds on the dynamic response. The model of Equations 3 and 4 is useful for such analyses provided that shear strains are below a limit of approximately 1.5 to 2.0, depending on the rubber compound. Beyond this limit the bearings exhibit stiffening behavior with tangent stiffness approximately equal to twice the tangent stiffness prior to initiation of stiffening. The interested reader is referred to Tsopelas *et al.*[7] for a model with stiffening behavior at large strains.

To illustrate the establishment of model parameters from test data of prototype bearings, Figure 7 shows experimentally determined properties of the high damping rubber bearing of which loops are shown in Figure 6. These properties are the tangent shear modulus, $G$, and the equivalent damping ratio, $\xi$ (defined as the energy dissipated in a cycle of motion divided by $4\pi$ and by the maximum kinetic energy) under scragged conditions. With reference to Figure 2, $G$, is related to the post-yielding stiffness $K_p$.

$$K_p = \frac{GA_r}{\Sigma t} \tag{7}$$

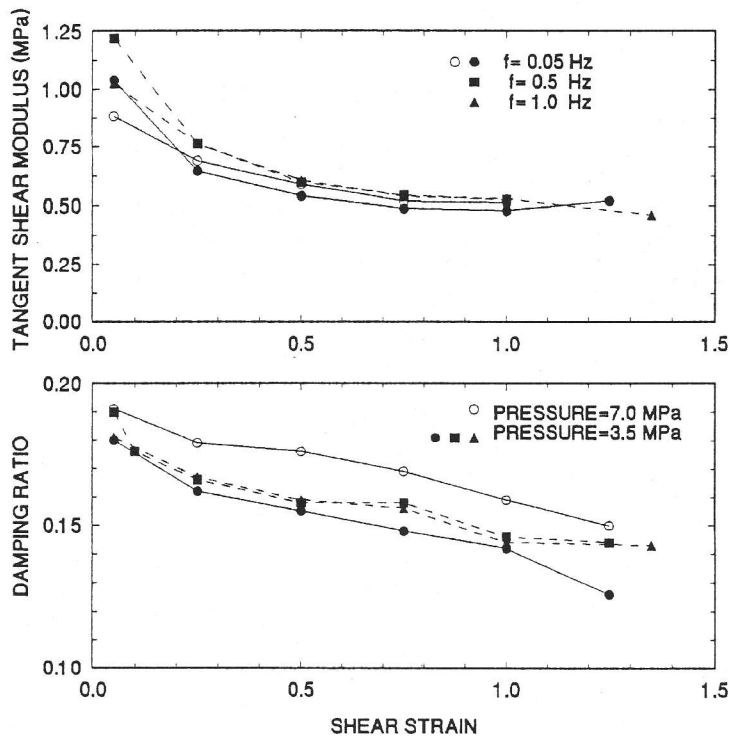


**Figure 7.** Mechanical properties of high damping rubber bearing.

where $A_r$ = bonded rubber area. The results of Figure 7 demonstrate that the tangent shear modulus and equivalent damping ratio are only marginally affected by either the frequency of loading or the bearing pressure, within the indicated range. Moreover, the bearings exhibit a high damping ratio.

The parameters of the model of Equations 3 and 4 may be determined by use of the mechanical properties of $G$ and $\xi$ at a specific strain, say the one corresponding to the design displacement $D$. The post-yielding stiffness $K_p$ is determined from Equation 7, whereas the characteristic strength, $Q$, may be related to the mechanical properties by assuming bilinear hysteretic behavior:

$$Q = \frac{\pi \xi K_p D^2}{(2 - \pi \xi) D - 2D_y} \tag{8}$$

where the yield displacement $D_y$ is between 0.05 and 0.1 times the total

rubber thickness. The yield force, $F^y$, is given by

$$F^y = Q + K_p D_y \tag{9}$$

and the post to pre-yielding stiffness ratio is given by

$$\alpha = \frac{K_p D_y}{F^y} \tag{10}$$

The mechanical properties at shear strain of 1.0 and bearing pressure of 7.0 MPa are $G = 0.50$ MPa and $\xi = 0.16$. For the small scale bearing of which the experimental loops are shown in Figure 5, $A_r = 52258$ mm$^2$, $\Sigma t = 8.25$ mm so that $K_p = 316.7$ N/mm, $Q = 10123$N (for $D_y = 0.10\ \Sigma t = 8.25$ mm), $F^y = 12736$N and $\alpha = 0.205$. The experimental loops of force vs displacement can now be simulated by using the model of Equations 3 and 4, with $A = 1$ and $\beta = \gamma = 0.5$. The simulated loops are shown in Figure 8, where it may be observed that the loop at shear strain of 1.0 agrees well with the corresponding experimental one. However, the analytical loops at lower peak shear strain have constant characteristic strength, whereas the experimental ones have a strength dependent on the amplitude of strain. Nevertheless, the model produces acceptable results on the peak response of an isolated structure when its calibration is based on the mechanical properties at a strain corresponding to the design displacement.

### 1.2.2. Sliding Bearings

Sliding bearings limit the transmission of force to the isolated structure to a predetermined level. While this is desirable, the lack of restoring force results in significant dispersion in the peak displacement response and results in the development of permanent displacements. To avoid these undesirable features sliding bearings should be used in combination with a restoring force mechanism. One of the simplest ways to introduce restoring force is by providing a spherical sliding surface as in the Friction Pendulum or FPS bearings.[3,11–13]

Figure 9 shows a cross-sectional view of an FPS bearing, whereas Figure 10 shows a view of a disassembled and of an assembled small scale FPS bearings in the laboratory of the authors. The sliding surface is spherical with radius of curvature $R$. Tsopelas *et al.*[7,13] modeled the behavior of FPS bearings using Equation 4 with yield displacement $D_y$ being very small (typically less than 2 mm) and

$$F_x = \frac{N}{R} U_x + \mu_s N Z_x, \qquad F_y = \frac{N}{R} U_y + \mu_s N Z_y, \tag{11}$$

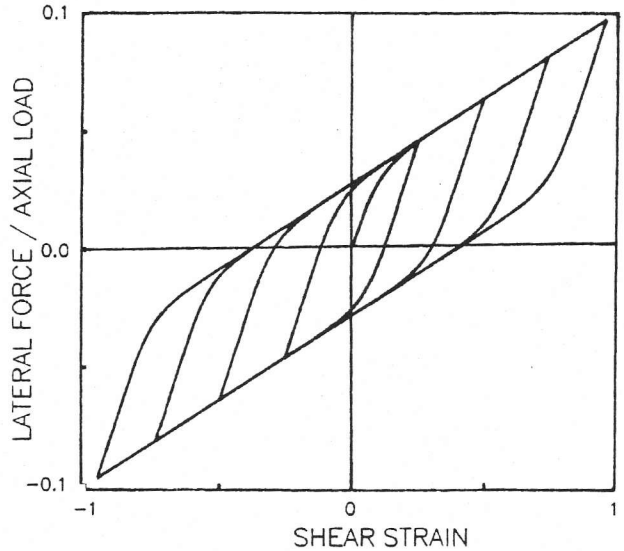


**Figure 8.** Analytically predicted force-displacement loops of high damping rubber bearing.

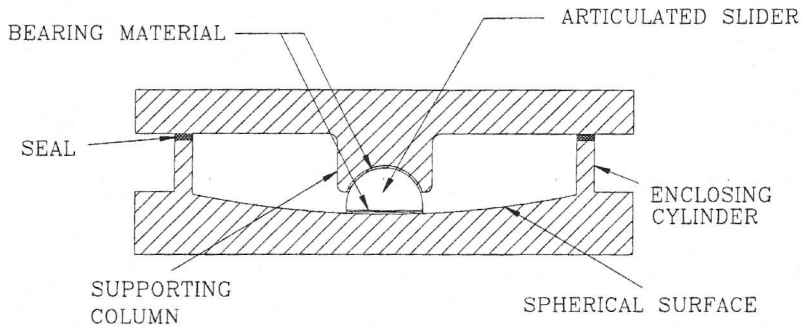


**Figure 9.** Cross section view of Friction Pendulum (FPS) bearing.

where $\mu_s$ is the coefficient of sliding friction and $N$ is the normal load on the bearing. The normal load consists of the gravity load, $W$, the effect of vertical ground acceleration, $\ddot{U}_v$, and the additional seismic load $P_s$ due to overturning moment:

$$N = W\left(1 + \frac{\ddot{U}_v}{g} + \frac{P_s}{W}\right) \tag{12}$$

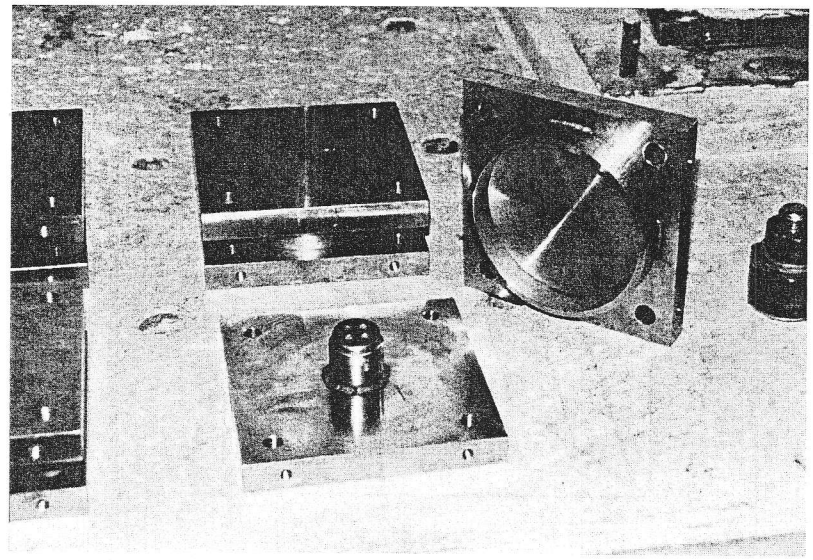

**Figure 10.** Views of assembled and disassembled small scale FPS bearings.

where $g$ is the acceleration of gravity. It should be noted that for flat sliding bearings $R$ is infinite and Equations 11 collapse to the model described in Constantinou *et al.*[9] which was experimentally verified by Mokha *et al.*[14]

The coefficient of friction of sliding bearings depends on a number of parameters, of which the composition of the sliding interface, bearing pressure and velocity of sliding are the most important. For interfaces consisting of polished stainless steel in contact with PTFE or PTFE-based composites, the coefficient of friction may be described by[3,7,9]:

$$\mu_s = f_{\max} - (f_{\max} - F_{\min}) \exp(-a|\dot{U}|) \tag{13}$$

where

$$\dot{U} = (\dot{U}_x^2 + \dot{U}_y^2)^{1/2} \tag{14}$$

is the magnitude of the instantaneous velocity. Parameters $f_{\min}$ and $f_{\max}$ describe, respectively, the coefficient of friction at essentially zero and large velocities of sliding and under constant pressure, as depict in Figure 11. Parameters $f_{\max}$, $f_{\min}$ and $a$ depend on the bearing pressure, although the writers found only the dependency of $f_{\max}$ on pressure to be of some practical significance. A relation found to approximate well experimental data[13] is

$$F_{\max} = f_{\max\ o} - (f_{\max\ o} - f_{\max\ p}) \tanh(\varepsilon p) \tag{15}$$

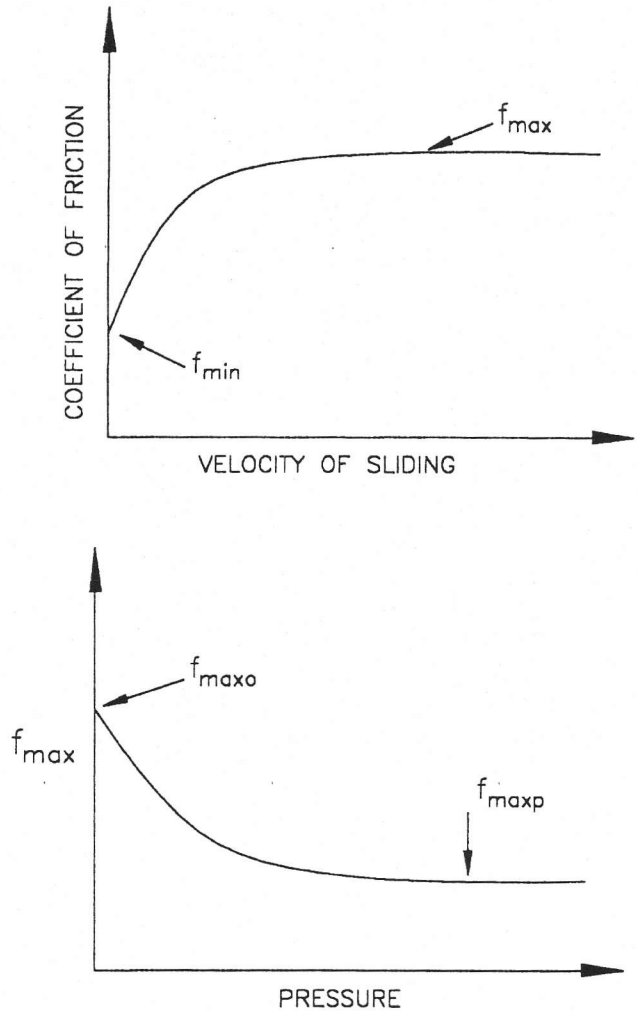


**Figure 11.** Dependency of coefficient of friction on velocity and pressure.

where the physical significance of parameters $f_{\max\ o}$ and $f_{\max\ p}$ is illustrated in Figure 11. Moreover, $p$ is the instantaneous bearing pressure, which is equal to the normal load $N$ (Equation 12) divided by the contact area.

Al-Hussaini *et al.*[12] reported shake tests results of a 7-story quarter length scale structure supported by eight FPS bearings. The structure had a weight of 212 kN and the bearings had radius of curvature $R = 248$ mm and

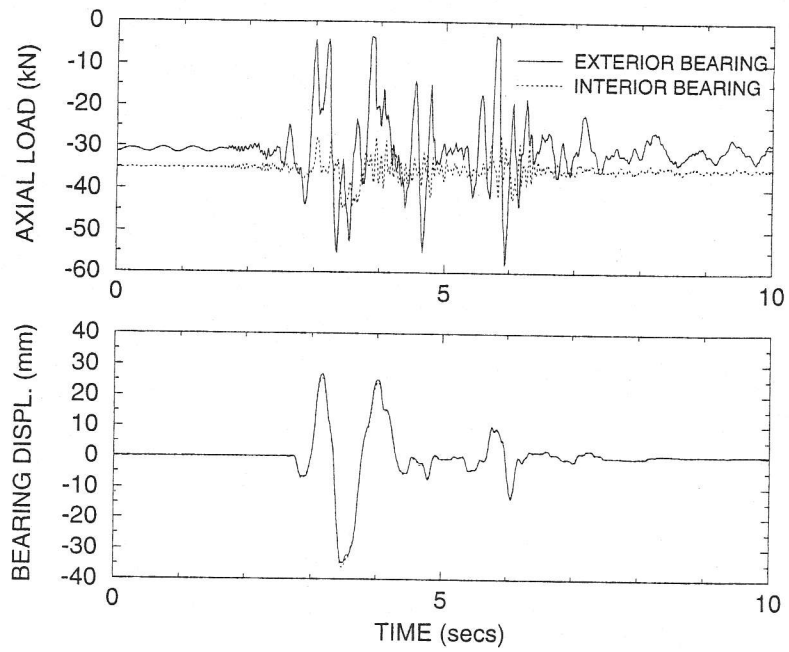


**Figure 12.** Histories of axial load and horizontal displacement of tested FPS bearings.

parameters $f_{\max o} = 0.12$, $f_{\max p} = 0.05$, $f_{\min} = 0.04$, $\varepsilon = 0.012\ (\mathrm{MPa})^{-1}$ and $a = 0.0429$ sec/mm. Under static conditions, one interior bearing was subjected to a pressure of about 220 MPa, whereas one exterior bearing was subjected to a pressure of 120 MPa. In a test with the 1971 San Fernando earthquake, record at Pacoima Dam, component S74W, the bearings were subject to the displacement and axial force histories shown in Figure 12. The significant variation of the axial load should be noted. The recorded and analytically predicted bearing force-displacement loops are shown in Figure 13, where the analytical prediction is seen to be very good.

### 1.2.3. Fluid Dampers

Fluid dampers are devices for dissipating energy. They may be classified into viscous shear dampers and inertial fluid dampers depending on their operating design. Viscous shear dampers or viscoelastic fluid dampers operate

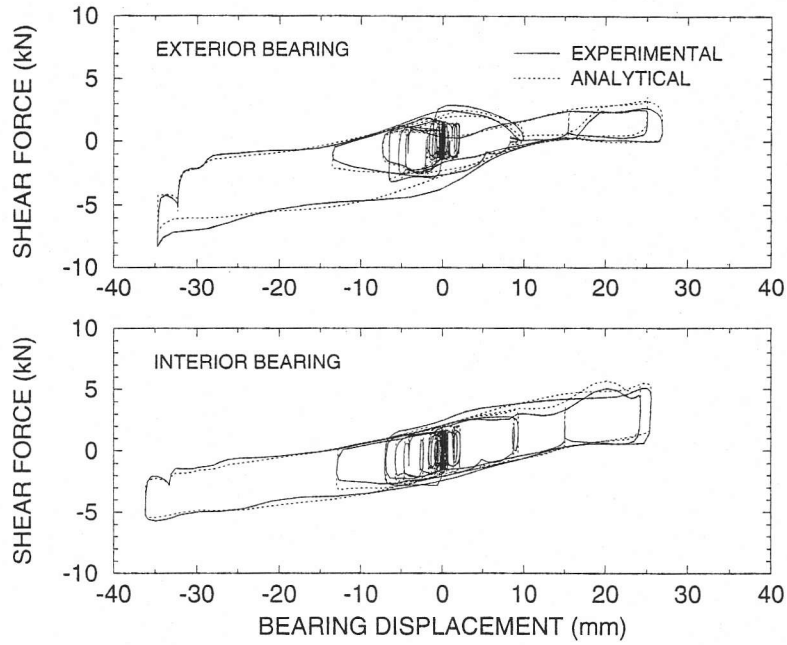


**Figure 13.** Comparison of analytical and experimental force-displacement loops of tested FPS bearings.

on the principle of shearing and deformation of highly viscous fluids.[15] These fluids, e.g., silicone gel, exhibit strong viscoelastic behavior (that is, they exhibit significant stiffness in addition to damping) so that their mechanical characteristics, and those of the damper, are strongly dependent on frequency and temperature. Moreover, they operate at low pressures (less than 2 MPa), making these devices rather large for the level required of output force. Makris *et al.*[15,16] developed analytical models for viscoelastic fluid dampers in the form of the fractional Maxwell model:

$$F + \lambda \frac{d^q F}{dt^q} = C_o \frac{dU}{dt} \tag{16}$$

where $F$ is the force produced by the damper, $U$ is the displacement and $q$ is the order of differentiation in the range (0,1). However, it is acceptable to model the damper by the Kelvin model when the response of the structure contains frequencies within a narrow band, centered at a frequency $\Omega$:

$$F = K_1(\Omega)U + C(\Omega)\frac{dU}{dt} \tag{17}$$

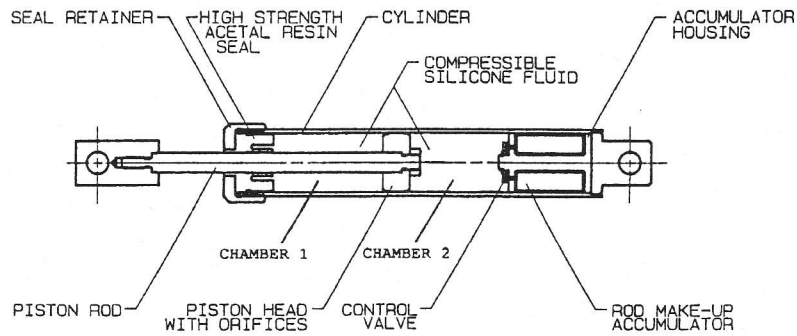


**Figure 14.** Construction of fluid inertial viscous damper.

where $K_1$ and $C$ are, respectively, the storage stiffness and damping coefficient of the device at frequency $\Omega$.

Inertial fluid dampers produce force by forcing fluid (typically silicone oil) through orifice passages.[3,17,18] The force depends on the size and shape of the orifices. Figure 14 shows the construction of a fluid inertial damper. The force acting on the piston is the product of pressure differential across the piston head and rod area. Operating pressures of 15 to 70 MPa are common, thus minimizing the effect of fluid viscosity, since high inertial fluid pressures dominate the output. A lengthy description of the construction and behavior of inertial fluid dampers may be found in Soong and Constantinou.[3] Herein it is sufficient to mention that it is possible to shape the orifice passages in such a way as to produce an output force of the type

$$F = C|\dot{U}|^{\alpha}\mathrm{sgn}(\dot{U}) \tag{18}$$

where $\alpha$ is in the range of 0.3 to 1.2. Of significance in seismic applications are devices with parameter $\alpha$ equal to unity (linear viscous dampers) or less. The latter are useful in applications of high velocity seismic input. A notable example of application are the 184 nonlinear ($\alpha = 0.3$) inertial fluid dampers in the isolation system of the San Bernardino County Medical Center in California.[19] Each of these dampers has 3.75 m length, stroke of $\pm 0.6$ m and output force of 1425 kN at velocity of 1.5 m/s. Taylor and Constantinou[20] tested reduced-scale prototypes of these dampers. Figure 15 shows the experimentally determined force-velocity relation at ambient temperature of 0 to 49°C. The solid line shows the analytically constructed relation using Equation 18 with $C = 33$ kN(s/mm)$^{0.3}$ and $\alpha = 0.3$. The insensitivity of properties of the device to ambient temperature, which was a requirement for this project, was accomplished by proper selection of materials and material

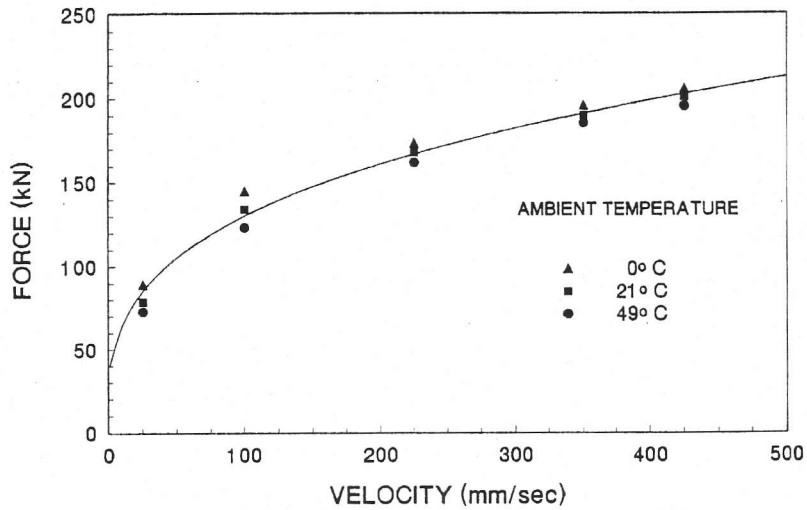


**Figure 15.** Constitutive relation of tested scaled fluid damper for San Bernardino County Medical Center.

volumes so that physical changes in the physical and mechanical properties of the fluid were compensated by volume changes so that fluid pressures were practically unaffected.

## 1.3. DYNAMIC ANALYSIS OF SEISMICALLY ISOLATED STRUCTURES

For seismically isolated buildings it is common to perform analysis assuming elastic behavior of the superstructure, that is, the part above the isolation system. A formulation of the problem of calculating the time history of dynamic response of isolated structures has been incorporated in the class of computer programs 3D-BASIS.[5–7] The equations of motion of the elastic superstructure are written in the form

$$\mathbf{M}\ddot{\mathbf{U}} + \mathbf{C}\dot{\mathbf{U}} + \mathbf{K}\mathbf{U} = -\mathbf{M}\mathbf{R}(\ddot{\mathbf{U}}_b + \ddot{\mathbf{U}}_g) \tag{19}$$

where **M**, **C** and **K** are the combined mass, damping and stiffness matrices of the superstructure (may consist of a single building or multiple buildings), **U** is the vector of displacements with respect to the isolation basemat, $\ddot{\mathbf{U}}_g$ is the ground acceleration vector, $\mathbf{U}_b$ is the displacement vector of the center of

mass of the isolation basemat with respect to the ground, **R** is a transformation matrix and a dot denotes differentiation with respect to time. The equation of motion of the isolation basemat is given by

$$\mathbf{R}^{\mathbf{T}}\mathbf{M}\{\ddot{\mathbf{U}} + \mathbf{R}(\ddot{\mathbf{U}}_{\mathbf{b}} + \ddot{\mathbf{U}}_{\mathbf{g}})\} + \mathbf{M}_{\mathbf{b}}(\ddot{\mathbf{U}}_{\mathbf{b}} + \ddot{\mathbf{U}}_{\mathbf{g}}) + \mathbf{f} = \mathbf{0} \tag{20}$$

in which $\mathbf{M_b}$ is the mass matrix of the isolation basemat and **f** is a vector containing the forces mobilized in the isolation elements. These forces are related to the state of motion of the isolation basemat, which is described by vector $\mathbf{U_b}$ and Equations 3, 4, 11, 17 and 18, and the location of each isolation element. These equations are easily solved by first reducing Equations 19 and 20 to first order form and then integrating using a predictor-corrector scheme. Alternatively, the equations may be solved by treating vector **f** in Equation 20 as a known load vector, solve the remaining linear equations and then update the estimate on the vector $f$ in an iterative procedure. The latter approach has been followed in the class of computer programs 3D-BASIS.

### 1.3.1. Analysis of a LNG Storage Tank Facility

The LNG storage tanks in Greece (Figure 2) were analyzed using computer code 3D-BASIS-ME. Figure 16 shows the geometry of one of these tanks and the layout of the 212 isolation bearings. These bearings are of the FPS type (Figure 9) with radius of curvature $R = 1.88$ m. A mathematical representation of the structure, which was used in calculating displacement demands for the bearings, is illustrated in Figure 17. In this model, the superstructure is modeled by three simple systems which, respectively, represent the outer concrete tank, the steel-tank system and the sloshing fluid. This model is valid in the horizontal plane. A different representation was employed in the vertical direction in order to represent the vertical flexibilities of the superstructure.

Each isolation bearing was explicitly modeled in accordance with the layout of Figure 16. Pressure and velocity dependencies of the coefficient of sliding friction were modeled in accordance with Equations 13 and 15 (see also Figure 11). Moreover, each bearing model was assigned randomly selected parameters within a range consistent with experimental data so that, on the average, the coefficient of friction was the least expected during the lifetime of the facility. Analyses were performed with a number of scaled earthquakes that were representative of the seismicity of the site for a return period of 10,000 years. Each of these earthquakes included two horizontal and one vertical components.

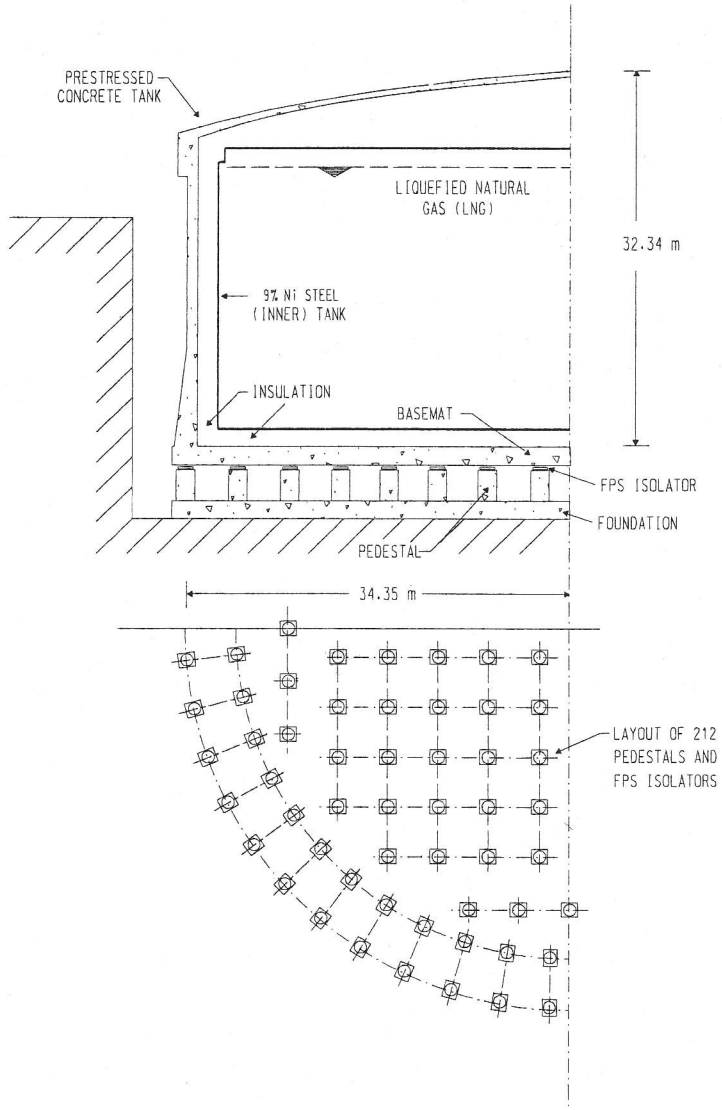


**Figure 16.** Geometry of isolated LNG storage facility.

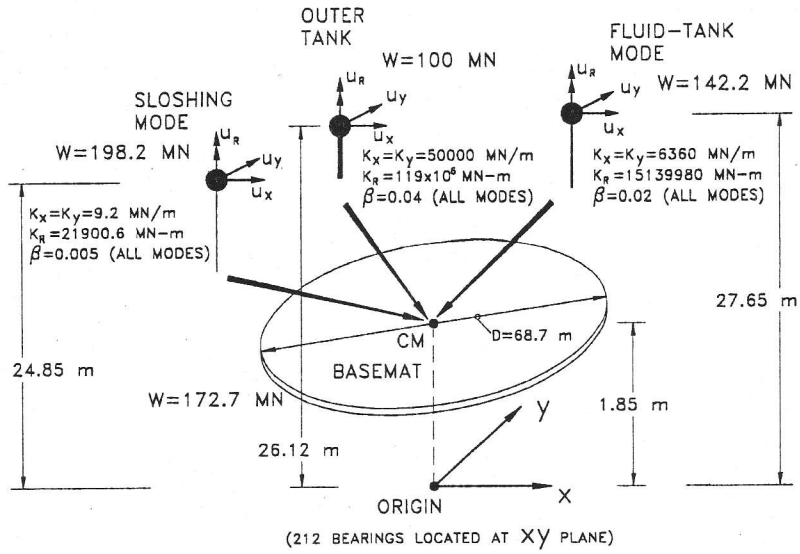


**Figure 17.** Mathematical representation of isolated LNG facility for calculation of bearing displacement demands.

Figure 18 shows a representative result from these analyses. The figure shows the displacement orbit calculated for an exterior bearing in one of the scaled earthquakes. It may be seen in this figure that the bearing displacement is primarily along a single direction, that is, the direction of strongest horizontal earthquake component.

### 1.3.2. Analysis of a Building Complex

Long buildings are usually separated by joints which allow thermal and moisture movements to occur without overstressing masonry walls. Figure 19 shows the layout of one such building complex. It consists of four six-story buildings separated by expansion joints of 50 mm width. The four buildings are supported by 153 lead-rubber bearings with the properties listed in Table 1. The basemats of these four buildings are connected together at the isolation system level forming a large T-shaped basemat.

At the time of analysis and design of this structure, the capability of dynamic analysis of an isolated building complex was not readily available to the structural engineering community. Accordingly, each building was

**Table 1.** Properties of Lead/Rubber Bearings

| | Bearing type | | | |
|---|---|---|---|---|
| | A | B | C | D |
| Dimensions (mm) | 380 × 380 | 460 × 460 | 540 ×540 | 530 × 530 |
| Bearing height (mm) | 220.00 | 220.00 | 220.00 | 220.00 |
| Lead core diameter (mm) | 70.00 | 100.00 | 90.00 | 0.00 |
| No. of rubber layers | 13.00 | 13.00 | 13.00 | 13.00 |
| Rubber layer thickness (mm) | 9.50 | 9.50 | 9.50 | 9.50 |
| Characteristic strength (kN) | 30.22 | 64.11 | 49.06 | 0.00 |
| Yield displacement (mm) | 5.23 | 7.06 | 4.35 | 1.00 |
| Post yielding stiffness (kN/mm) | 1.05 | 1.66 | 2.05 | 1.15 |
| No. of bearings in part III | 19.00 | 3.00 | 10.00 | 0.00 |
| No. of bearings in complex | 55.00 | 25.00 | 61.00 | 12.00 |

**Table 2.** Calculated Maximum Response of Part III of Isolated Building Complex

| | | Complex | | Individual | |
|---|---|---|---|---|---|
| Direction of ground motion | | X | | Y | |
| Response direction | | X | Y | X | Y |
| Structure shear / weight | | 0.240 | 0.023 | 0.181 | 0.001 |
| Peak floor | 6 | 0.284 | 0.044 | 0.228 | 0.003 |
| acceleration at C.M. | 5 | 0.261 | 0.038 | 0.206 | 0.002 |
| (g) | 4 | 0.248 | 0.026 | 0.189 | 0.001 |
| | 3 | 0.233 | 0.022 | 0.186 | 0.001 |
| | 2 | 0.216 | 0.015 | 0.194 | 0.002 |
| | 1 | 0.205 | 0.012 | 0.197 | 0.001 |
| Peak interstory drift ratio | 6 | 0.122 | 0.012 | 0.097 | 0.010 |
| at corner column | 5 | 0.128 | 0.013 | 0.102 | 0.011 |
| (% of column height) | 4 | 0.129 | 0.012 | 0.102 | 0.010 |
| | 3 | 0.126 | 0.013 | 0.098 | 0.009 |
| | 2 | 0.100 | 0.012 | 0.079 | 0.009 |
| | 1 | 0.050 | 0.005 | 0.039 | 0.003 |
| Corner bearing peak displacement (mm) | | 128.00 | 3 | 133.00 | 3 |

is neglected (analysis as individual part). The reason for this difference is torsional response of the complex which tends to amplify the response at the farthest located columns from the center of mass of the basemat. Despite these differences, the design of the isolation system fulfilled all requirements of this project and there was no need for redesign of the isolation system. This complex was the first hospital facility to be designed as seismically isolated in 1988. However, the project was canceled and the hospital was never built.

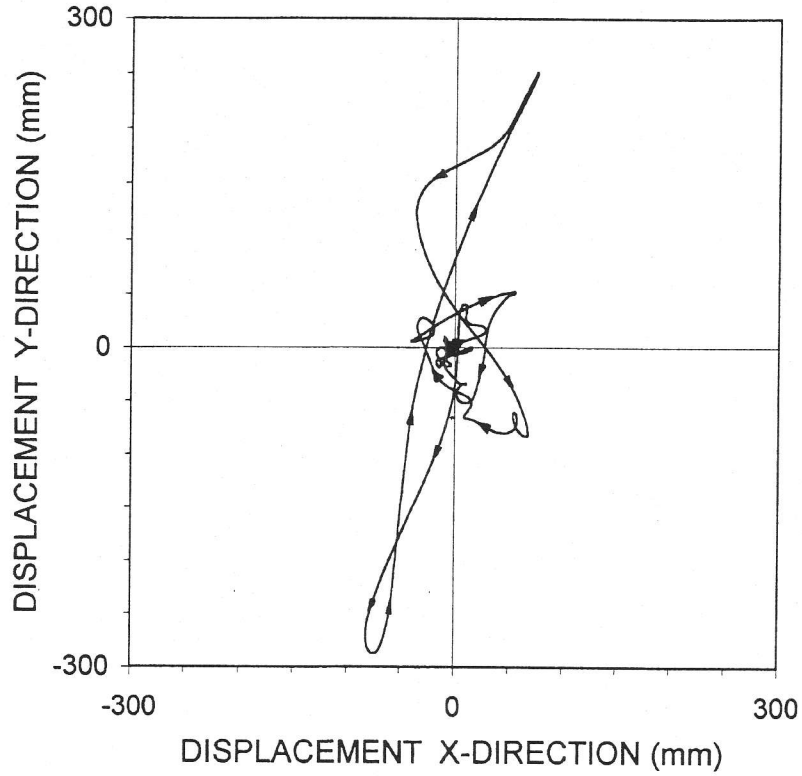


**Figure 18.** Calculated displacement orbit of exterior bearing of LNG storage facility.

analyzed individually without accounting for interaction between the interconnected buildings. Analysis capability became available when computer code 3D-BASIS-M (a precedent to code 3D-BASIS-ME) was developed by Tsopelas *et al.*[21] Dynamic analysis of the isolated building complex was performed and representative results are presented in Table 2. The complex was analyzed for a particular earthquake component applied in the X direction as shown in Figure 19. The calculated peak response of part III is presented in Table 2. Moreover, part III was analyzed alone without due account given to the interaction with adjacent parts. This calculated response is also presented in Table 2.

It may be observed in this table that the response of part III of this structure is affected by interaction with adjacent parts. Particularly, the superstructure acceleration, shear force and drift response of part III is larger when interaction is accounted for (analysis as complex) than when interaction

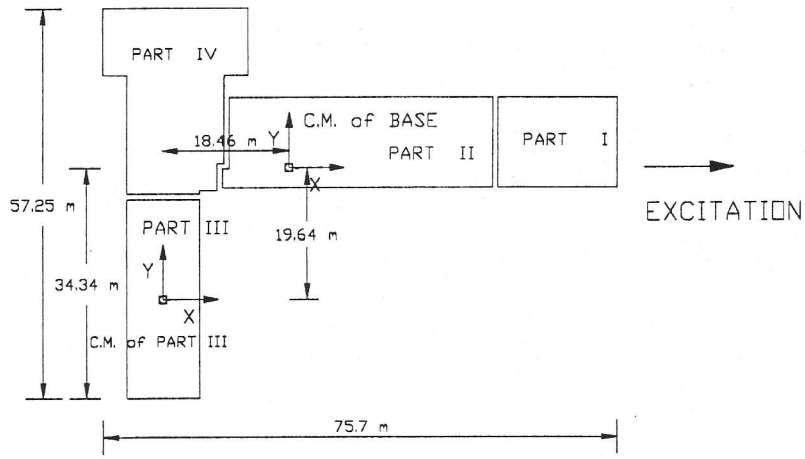


**Figure 19.** Layout of isolated four-building hospital complex.

## 1.4. CONCLUSIONS

Seismic isolation has reached sufficient level of maturity so that widespread application can be expected. The development of the class of computer codes 3D-BASIS has been instrumental in the advancement of this design approach from theory to practice. While these computer programs were originally developed for research purposes, they were made available to the profession and have been widely used in the dynamic analysis of seismically isolated structures. Commercial computer programs, such as ETABS V.6 of Computer and Structures, Inc. of Berkeley, California, have been recently modified to include capabilities for analysis of seismically isolated structures. This represents another significant step towards the application of seismic isolation.

### References

1. Skinner, R.I., W.H. Johnson and G.H. McVerry, 1993, *An Introduction to Seismic Isolation*, J. Wiley & Sons, New York.
2. Kelly, J.M. 1993, *Earthquake-Resistant Design with Rubber*, Springer-Verlag, New York.
3. Soong, T.T. and M.C. Constantinou, 1994, *Passive and Active Structural Vibration Control in Civil Engineering*, Springer-Verlag, Wien and New York.
4. Mokha, A.S., N. Amin, M.C. Constantinou and V. Zayas, 1996, *J. Struct. Engng., ASCE*, **122**(3), 298–308.

5. Nagarajaiah, S., A.M. Reinhorn and M.C. Constantinou, 1991, *3D-BASIS Nonlinear Dynamic Analysis of Three-Dimensional Base Isolated Structures: Part II*, Report No. 91-0005, National Center for Earthquake Engineering Research, Buffalo, NY.
6. Reinhorn, A.M., S. Nagarajaiah, M.C. Constantinou, P. Tsopelas and R. Li, 1994, *3D-BASIS-TABS: Version 2.0 Computer Program for Nonlinear Dynamic Analysis of Three Dimensional Base Isolated Structures*, Report No. 94-0018, National Center for Earthquake Engineering Research, Buffalo, NY.
7. Tsopelas, P.C., M.C. Constantinou and A.M. Reinhorn, 1994, *3D-BASIS-ME: Computer Program for Nonlinear Dynamic Analysis of Seismically Isolated Single and Multiple Structures and Liquid Storage Tanks*, Report No. 94-0010, (National Center for Earthquake Engineering Research, Buffalo, NY.
8. Park, Y.J., Y.K. Wen and A.H.S. Ang, 1986, *Earthquake Engrg. Struct. Dyn.*, **14**(4), 543–557.
9. Constantinou, M.C., A.M. Mokha and A.M. Reinhorn, 1990, *J. Struct. Engng., ASCE*, **116**(2), 455–474.
10. Muroto, N., K. Goda, S. Suzusi, C. Sudo and Y. Suizu, 1994, *Proc. 3rd U.S.-Japan Workshop on Earthquake Protective Systems for Bridges*, National Center for Earthquake Engineering Research, Report No. 94-0009, Buffalo, NY., pp. 2–63 to 2–76.
11. Mokha, A., M.C. Constantinou, A.M. Reinhorn and V. Zayas, 1991, *J. Struct. Engng., ASCE*, **117**(4), 1201–1217.
12. Al-Hussaini, T., V. Zayas and M.C. Constantinou, 1994, *Seismic Isolation of Multi-Story Frame Structures Using Spherical Sliding Isolation System*, Report No. 94-0007, National Center for Earthquake Engineering Research, Buffalo, NY.
13. Tsopelas, P., M.C. Constantinou, Y.S. Kim and S. Okamoto, 1996, *Earthquake Engng. Struct. Dyn.*, **25**(1), 65–78.
14. Mokha, A.S., M.C. Constantinou and A.M. Reinhorn, 1993, *J. Struct. Engrg., ASCE*, **119**(1), 240–261.
15. Makris, N., M.C. Constantinou and G.F. Dargush, 1993, *J. Struct. Engng., ASCE*, **119**(11), 3310–3325.
16. Makris, N., G.F. Dargush and M.C. Constantinou, (1995), *J. Engng. Mechanics, ASCE*, **121**(10), 1114–1121.
17. Constantinou, M.C. and M.D. Symans, 1992, *Experimental and Analytical Investigatoin of Seismic Response of Structures with Supplemental Fluid Viscous Dampers*, Report No. 92-0032, National Center for Earthquake Engineering Research, Buffalo, NY.
18. Constantinou, M.C., T.T. Soong and G.F. Dargush, 1996, *Passive Energy Dissipation Systems for Structural Design and Retrofit*, National Center for Earthquake Engineering Research, Buffalo, NY.
19. Rosenbaum, D.B., 1995, *Engineering News-Record*, pp. 24–26.
20. Taylor, D.P. and M.C. Constantinou, 1995, *Shock and Vibration* **2**(5), 373–381.
21. Tsopelas, P., S. Nagarajaiah, M.C. Constantinou and A.M. Reinhorn, 1994, *Computers and Structures*, **50**(1), 47–57.